BULLETIN DE L'ASSOCIATION MINERALOGIQUE DU CANADA

THE CANADIAN MINERALOGIST

JOURNAL OF THE MINERALOGICAL ASSOCIATION OF CANADA

Volume 33 October 1995 Part 5

The Canadian Mineralogist
Vol. 33, pp. 949-960 (1995)

S K- AND L-EDGE X-RAY ABSORPTION SPECTROSCOPY OF METAL SULFIDES AND SULFATES: APPLICATIONS IN MINERALOGY AND GEOCHEMISTRY

DIEN LI, G. MICHAEL BANCROFT AND MASOUD KASRAI

Department of Chemistry, The University of Western Ontario, London, Ontario N6A 5B7

MICHAEL E. FLEET*

Department of Earth Sciences, The University of Western Ontario, London, Ontario N6A 5B7

XINGHONG FENG AND KIM TAN

Canadian Synchrotron Radiation Facility, Synchrotron Radiation Center, University of Wisconsin, Stoughton, Wisconsin 53589, U.S.A.

ABSTRACT

S *K*- and *L*-edge XANES spectra of pyrrhotite ($Fe_{1-x}S$), pyrite (FeS_2), the thiospinels carrollite ($CuCo_2S_4$) and linnaeite (Co_3S_4), and Mg, Ca, Sr and Ba sulfates have been obtained using synchrotron radiation. The spectra of these metal sulfides are interpreted based on qualitative molecular orbital (MO) – energy-band models, and indicate that the metal 3*d* crystal-field band below the conduction band minimum has significant S 3*s*- and 3*p*-like density of states (DOS), because of strong participation of the metal 3*d* electrons in the bonding of the metals with sulfur. The S *K*- and *L*-edge spectra of sulfates are interpreted using MO theory. The S *K*- and *L*-edges shift to higher energy by about 10 eV from sulfides (S^{2-}) to sulfur (S^0), sulfite (S^{4+}) and sulfates (S^{6+}), providing a powerful and independent technique for the determination of oxidation state of sulfur. For semiconducting metal sulfides, the S *K*- and *L*-edges shift linearly to higher energy by 2–3 eV with increase in the energy band gap (E_g), and curvilinearly to lower energy with increase in reflectivity.

Keywords: X-ray absorption spectroscopy, sulfides, sulfates, oxidation state of sulfur, energy band-gap.

SOMMAIRE

Nous avons obtenu des spectres d'absorption X (XANES) aux seuils *K* et *L* du soufre pour la pyrrhotite ($Fe_{1-x}S$), pyrite (FeS_2), les thiospinelles carrollite ($CuCo_2S_4$) et linnaeïte (Co_3S_4), ainsi que pour les sulfates de Mg, Ca, Sr et Ba, en utilisant une source de rayonnement synchrotron. Nous interprétons le spectre de ces sulfures de métaux à la lumière de modèles qualitatifs de l'énergie des orbites moléculaires. D'après ces spectres, la bande de l'orbite 3*d* des atomes métalliques, d'un niveau

* To whom correspondence should be addressed.

d'énergie inférieur à celui de la bande de conduction, contient une contribution importante des densités d'états semblables aux orbites 3*s* et 3*p* du soufre, à cause d'une participation importante des électrons 3*d* des métaux dans les liaisons de ces métaux avec le soufre. Nous interprétons aussi les spectres d'absorption aux seuils *K* et *L* des sulfates en utilisant le modèle des orbites moléculaires. Les absorptions aux seuils *K* et *L* du soufre sont décalées vers une énergie plus élevée par environ 10 eV en passant de sulfures (S^{2-}) au soufre (S^0), sulfite (S^{4+}) et sulfate (S^{6+}). Cette technique constituerait donc un outil puissant et indépendant dans la détermination de l'état d'oxydation du soufre. Dans le cas des sulfures métalliques semiconducteurs, les absorptions aux seuils *K* et *L* du soufre sont décalés de façon linéaire vers une énergie plus élevée par 2–3 eV avec une augmentation en énergie dans la séparation des bandes (E_g), et de façon "curvilinéaire" vers une énergie plus faible avec une augmentation dans la réflectivité.

(Traduit par la Rédaction)

Mots-clés: spectroscopie d'absorption des rayons X, sulfures, sulfates, oxydation du soufre, séparation énergétique des bandes.

Introduction

The first X-ray absorption spectrum (XAS) was reported by Kossel (1920). However, XAS was not as widely used as X-ray diffraction (XRD) in physics and chemistry because of difficulties in interpretation, limitations of exciting light sources, and the indirect and implicit nature of the structural information obtainable. In the early 1970s, bright and polarized synchrotron radiation, tunable over a wide range in photon energy, became available for XAS measurements, and a short-range single-electron scattering theory for EXAFS was developed (Sayers *et al.* 1970, Stern 1974, Sayers 1975). Since then, XAS has been applied in mineralogy and geochemistry, biology and material sciences, as well as physics and chemistry. XAS is element-specific and applicable to a wide selection of elements and density of states (DOS) components. It can be used to study gases, liquids, and crystalline and amorphous solids; it provides information on short-range structure and electronic structure, and it allows rapid acquisition of high-resolution spectra. XAS has been applied in mineralogy and geochemistry to determine the local geometrical arrangements of transition elements in silicates and oxides, electronic structure of metal sulfides, structures of amorphous materials, nucleation and crystallization of minerals in aqueous solutions, and mechanisms of chemisorption reactions at mineral–liquid interfaces. These and other applications of XAS in mineralogy and geochemistry have been reviewed in Calas *et al.* (1984, 1987), Brown *et al.* (1988, 1989), Brown & Parks (1989) and Brown (1990).

We have reported high-resolution S *K*- and *L*-edge X-ray absorption near-edge structure (XANES) of ZnS, $CuFeS_2$ and Cu_2FeSnS_4 (Li *et al.* 1994c), Zn, Cd and Hg monosulfides (Li *et al.* 1994a) and copper-containing sulfides (Li *et al.* 1994b), and investigated the unoccupied S 3*s*-, 3*p*- and 3*d*-like states in the conduction band of these sulfides. In this paper, we present and interpret S *K*- and *L*-edge XANES spectra of pyrrhotite and pyrite, carrollite and linnaeite, and Mg, Ca, Sr and Ba sulfates, and discuss various applications of these spectra.

Samples and Experimental Method

All mineral samples were obtained from the Department of Earth Sciences, University of Western Ontario, and the Department of Mineralogy, Royal Ontario Museum. Some sulfates investigated were analytical-grade reagents. All mineral samples were shown by powder X-ray diffraction (PXRD) and electron-microprobe analysis (EMPA) to be single-phase. The samples were finely ground in air to approximately 10 μm in size and spread uniformly on conducting carbon tape supported on a stainless-steel sample holder of about 15 mm in diameter for S *K*- and *L*-edge measurements. The S *K*-edge XANES spectra were collected with a Double-Crystal Monochromator (DCM) at a chamber pressure of about 10^{-6} torr and at room temperature, with 0.2 eV intervals and 2 seconds for each data point. The *K*-edge XANES spectra were calibrated using the *K*-edge of native sulfur at 2472.0 eV. The DCM used InSb (111) monochromator crystals and has an energy resolution of about 0.8 eV at 2460 eV; its detailed design and performance are described elsewhere (Yang *et al.* 1992).

The S *L*-edge XANES spectra were taken on the Grasshopper beamline (Bancroft 1992) at room temperature and chamber pressure of about 10^{-8} torr. The Grasshopper beamline uses grazing incidence with a grating of 1800 grooves/mm and has an energy resolution of about 0.2 eV at 160 eV. The spectra were calibrated by the first sharp peak at 162.7 eV in the *L*-edge spectrum of native sulfur.

All S *K*- and *L*-edge spectra were recorded by Total Electron Yield (TEY) and fluorescence modes as a function of photon energy using synchrotron radiation. The spectra recorded in these two modes were found to be very similar, and only the TEY spectra are presented here. The DCM and Grasshopper beamlines are affiliated with the Canadian Synchrotron Radiation Facility (CSRF) at the Aladdin storage ring, University of Wisconsin. The storage ring operates at either 800 MeV with a current of about 60–180 mA, or 1 GeV with a current of 40–80 mA.

RESULTS

Pyrrhotite

Figure 1 shows the S *K*- and *L*-edge XANES spectra of pyrrhotite, together with the Fe *K*-edge spectrum of synthetic $Fe_{1-x}S$. The S *L*-edge spectrum was aligned to zero by subtracting the S $2p_{3/2}$ binding energy (BE) of FeS at 161.2 eV, and the S *K*- and *L*-edge spectra are correlated using the S $K\alpha_1$ X-ray-emission energy at 2307.8 eV. The Fe *K*-edge spectrum of $Fe_{1-x}S$ was digitized from Sugiura (1984), and aligned to zero by subtracting the Fe 1*s* BE calculated as the sum of the Fe $2p_{3/2}$ BE at 710.1 eV and $K\alpha_1$ X-ray emission energy at 6403.8 eV. The S *K*-edge spectrum of pyrrhotite is also similar to previous results (Sugiura *et al.* 1974, Sugiura 1981, Sugiura & Muramatsu 1985, Kitamura *et al.* 1988).

Pyrrhotite has a NiAs-type structure, in which each Fe atom is octahedrally coordinated by S, and each S atom is triangular-prismatically coordinated by six Fe atoms. The six Fe^{2+} $3d^6$ electrons in pyrrhotite have high-spin t_{2g}^4–e_g^2 configuration, so that the majority spin t_{2g}^{α} and e_g^{α} bands are filled, whereas the minority spin t_{2g}^{β} band is partly filled, and the minority spin e_g^{β} band is completely empty (Tossell 1977, Sakkopoulos *et al.* 1984). In the Fe *K*-edge spectrum, a weak peak **a**, usually called a pre-edge feature, is assigned to the transition of Fe 1*s* electrons to the unoccupied 3*d* orbitals (t_{2g}^{β} and e_g^{β}). This transition is formally forbidden by the quantum selection rules, but local distortion of the coordination octahedron around the Fe atom mixes the Fe 3*p* and 3*d* orbitals, and makes this Fe $1s \rightarrow 3d$ transition weakly allowed. Peak **a** in both S *K*- and *L*-edge spectra corresponds to peak **a** in the Fe *K*-edge spectrum within ±0.5 eV, and is assigned to transitions of S 1*s* and 2*p* electrons to S 3*p*- and 3*s*-like states, respectively, mixed into the unoccupied Fe 3*d* crystal-field bands in the band gap. Peak **c** in the S *K*-edge spectrum is assigned to transition of S 1*s* electrons to S 3*p*-like states. In the *L*-edge spectrum, peak **b** is due to the transition of S 2*p* electrons to S 3*s*-like states, and peaks **c** and $\mathbf{d}_1$ are attributed to transitions of S 2*p* electrons to t_{2g} and e_g bands split from empty S 3*d* states (Li *et al.* 1994c). These results indicate that the Fe 3*d* crystal-field band in the band gap is hybridized with S 3*p* and 3*s* states, and the conduction-band minimum is characterized by Fe *s*- and *p*-like states whose DOS are also hybridized with S 3*s*-, 3*p*- and even 3*d*-like states. This is contrary to the recent calculations of electronic bands of cubic and tetragonal FeS, which indicate that the Fe–S bond is mainly ionic with little covalent mixing (Welz & Rosenberg 1987).

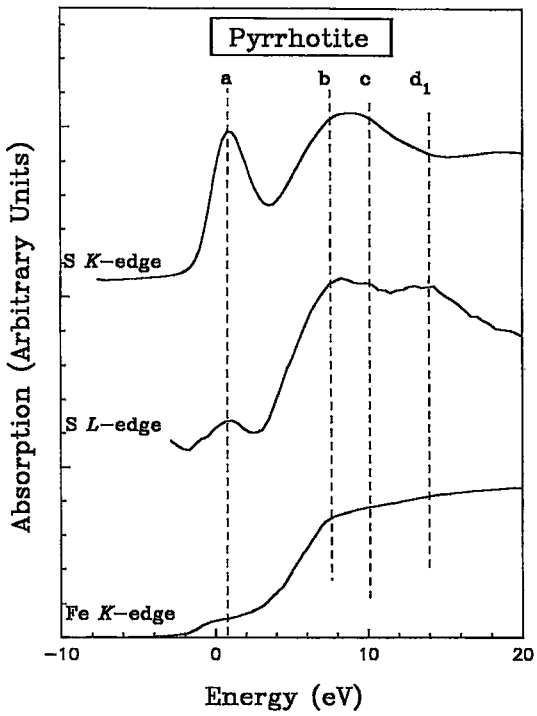

FIG. 1. S *K*- and *L*-edge XANES spectra of pyrrhotite, together with Fe *K*-edge spectrum. The S *K*- and *L*-edge spectra are aligned to zero energy by the S 1*s* and $2p_{3/2}$ BE (161.2 eV), respectively, where the S 1*s* BE is calculated from the sum of S $2p_{3/2}$ BE and S $K\alpha_1$ X-ray emission energy at 2307.8 eV. The Fe *K*-edge spectrum is aligned to zero by Fe 1*s* BE calculated by adding the Fe $2p_{3/1}$ BE of 710.1 eV and $K\alpha_1$ X-ray emission energy of 6403.8 eV.

Pyrite and marcasite

Figure 2 compares the S *K*- and *L*-edge XANES spectra of pyrite, and the Fe *K*-edge spectrum of FeS_2 digitized from Dräger *et al.* (1988). The S *L*-edge spectrum is aligned to zero by subtracting the S $2p_{3/2}$ BE at 162.4 eV (Hyland & Bancroft 1989), and the S *K*-edge spectrum is correlated with the *L*-edge spectrum by the S $K\alpha_1$ X-ray emission energy at 2307.8 eV. The Fe *K*-edge spectrum is aligned to zero using the Fe 1*s* BE calculated by adding Fe $2p_{3/2}$ BE at 706.5 eV and $K\alpha_1$ X-ray emission energy at 6304.8 eV. The partial DOS of S 3*p* and Fe 3*d* states in the first empty band of pyrite, digitized from Bullett (1982) and aligned by calibrating the Fermi level (E_F) to zero energy, are included for comparison. The S *K*- and *L*-edge spectra of native sulfur are also shown as dashed curves for comparison. Our results are in good agreement with previous work on pyrite (Sugiura 1981, Sugiura & Muramatsu 1985).

In the pyrite structure, each Fe atom is octahedrally coordinated by S atoms with an Fe–S distance of 2.26 Å, and each S atom bonds to another S atom

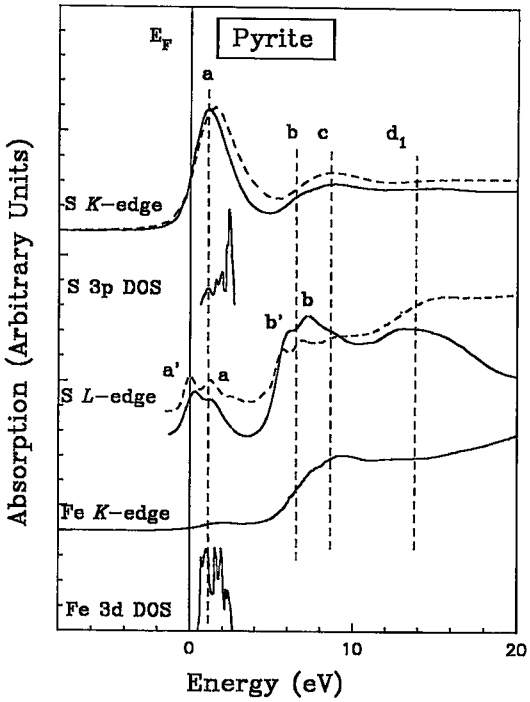

FIG. 2. S *K*- and *L*-edge XANES spectra of pyrite, together with Fe *K*-edge spectrum. The S *K*- and *L*-edge spectra are aligned to zero energy by the S 1s and $2p_{3/2}$ BE (162.4 eV), where the S 1*s* BE is calculated by the sum of the S $2p_{3/2}$ BE and S $K\alpha_1$ X-ray emission energy at 2307.8 eV. The Fe *K*-edge spectrum is aligned to zero by Fe 1*s* BE calculated from the sum of Fe $2p_{3/2}$ BE at 706.5 eV and Fe $K\alpha_1$ X-ray emission energy at 6403.8 eV. The calculated S 3*p* and Fe 3*d* DOS (Bullett 1982) are also included for comparison, by placing the Fermi level (E_F) at zero energy. The S *K*- and *L*-edge spectra of native sulfur (dash curves) are also compared to the corresponding spectra of pyrite.

at 2.08 Å and three Fe atoms. Pyrite is a semiconductor because the 3*d* crystal-field band lies in the band gap. The Fe^{2+} 3*d* electrons have low spin t_{2g}^6–e_g^0 configuration, and the filled t_{2g}^6 and empty e_g^0 bands are separated by about 0.7 eV, regarded as the indirect E_g of pyrite (Bullett 1982). On the other hand, there is no complete distinction between the antibonding S $p\sigma^*$ band and the empty Fe e_g^0 (3*d*) band, even though the former orbitals contribute principally at the top of the first unoccupied band (Goodenough 1972, Tossell *et al.* 1981, Bullett 1982). By comparison with the calculated DOS, peak **a** in the S *K*-edge spectrum is assigned to the transition of S 1*s* electrons to the S 3*p*-like states in the first unoccupied Fe e_g and S $p\sigma^*$ band, in agreement with Fe *K*-edge spectrum. Although the calculated DOS of the S *s*- and *d*-like states are not available, peak **a** in both S *K*- and *L*-edge spectra are aligned well within 0.4 eV, so that peak **a** in the S *L*-edge spectrum also seems be attributable to the transition of S 2*p* electrons to S 3*s*-like states in this empty band. Peak **b** in the S *L*-edge spectrum is assigned to the transition of S 2*p* electrons to the antibonding S 3*s*-like states at the conduction-band minimum, and peaks **c** and $\mathbf{d}_1$ are assigned to the empty S 3*d*-like e and t_2 states, respectively (Li *et al.* 1994c). Peaks **a** and **b** in the S *L*-edge spectrum are each split by 1.2 eV, owing to the spin-orbit interaction of S 2*p* orbitals. These results show that the first unoccupied state of pyrite is the Fe^{2+} crystal-field band strongly mixed with S 3*p*- and 3*s*-like states, and there is a strong overlap between the Fe *p*-like states and S 3*s*- and 3*p*-like states at the conduction-band minimum.

The S *K*- and *L*-edge spectra of marcasite, the other important polymorph of FeS_2, are very similar to those of pyrite, except for a shift of about 0.2 eV to lower energy, which is also in agreement with the electronic-structure calculation of pyrite- and marcasite-type sulfides (Bullett 1982). The S *K*- and *L*-edges of pyrite and pyrrhotite are very similar because they both have the FeS_6^{10-} cluster as the basic structural unit. However, there are two significant differences. First, peak **a** in the S *K*- and *L*-edge spectra of pyrite shifts to higher energy by about 1.5 eV. This mainly reflects the difference in Fe–S bond distances in pyrite and pyrrhotite. The MO-energy band calculation (Bullett 1982) indicates that the unoccupied Fe e_g sub-band is displaced to higher energy by about 1.2 eV because of the difference in Fe–S bond distance: 2.38 Å in monoclinic pyrrhotite *versus* 2.26 Å in pyrite, in good agreement with our S *K*- and *L*-edge spectra. Second, peak **a** is significantly more intense in the S *K*-edge spectrum of pyrite than in the spectrum of pyrrhotite; thus peak **a** is much more intense than peak **c** in pyrite, whereas peak **a** is somewhat weaker than peak **c** in pyrrhotite; also, peak **a** in the S *L*-edge spectrum of pyrite is more intense than in pyrrhotite. This indicates stronger mixing of S 3*s* and 3*p* states into the Fe 3*d* band in pyrite, which is apparently related to the presence of the S_2^{2-} ion, giving overlapping of the antibonding S $p\sigma^*$ band with the empty Fe e_g (3*d*) band. The similarity between the S *K*- and *L*-edge spectra of pyrite and native sulfur (Fig. 2) also supports this interpretation of the spectral features and emphasizes that the molecular S_2^{2-} ion is a dominant feature in the electronic structure of pyrite.

Carrollite and linnaeite

The S *K*- and *L*-edge XANES spectra of carrollite and linnaeite are similar, and only the carrollite spectra are shown in Figure 3, together with the Co and Cu *K*-edge spectra from the literature. The S *L*- and *K*-edge spectra are aligned to zero by the $2p_{3/2}$ BE at 162.3 eV (Nakai *et al.* 1978) and S 1*s* BE calculated by the sum of S $2p_{3/2}$ BE and S $K\alpha_1$ X-ray emission energy at

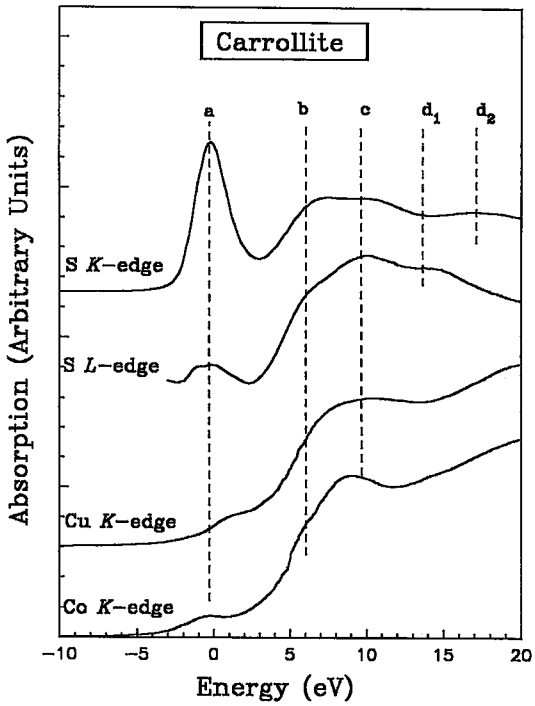

FIG. 3. S *K*- and *L*-edge XANES spectra of carrollite, together with Cu and Co *K*-edge spectra. The S *K*- and *L*-edge spectra are aligned to zero energy using S 1*s* and $2p_{3/2}$ BE (162.3 eV: Nakai *et al.* 1978), where the S 1*s* BE is calculated from the sum of the S $2p_{3/2}$ BE and S $K\alpha_1$ X-ray emission energy at 2307.8 eV. The Cu and Co *K*-edge spectra are digitized from Charnock *et al.* (1990), and re-aligned to our spectra by about 5 eV shifts to higher energy, because the main edges were taken as zero energy in Charnock *et al.* (1990).

2307.8 eV, respectively. The Co and Cu *K*-edge spectra are digitized from Charnock *et al.* (1990) and realigned with the S *K*- and *L*-edge spectra by an approximate 5 eV shift toward higher energy, because the main edge was taken as zero energy in Charnock *et al.* (1990).

Carrollite has the normal spinel structure, with low-spin Co^{3+} occupying half of the octahedral sites, and Cu^{2+} occupying one-eighth of the tetrahedral sites. The Co^{3+} at the octahedral sites has bonding (σ_B) and anti-bonding (σ_B^*) molecular orbitals formed by overlap of Co^{3+} e_g, 4*s* and 4*p* orbitals with S 3*s* and 3*p* orbitals. Filled t_{2g} orbitals probably remain essentially non-bonding. For Cu^{2+} at the tetrahedral sites, the e orbitals are non-bonding, whereas t_2, 4*s* and 4*p* orbitals form σ_A and σ_A^* bands (Tossell & Vaughan 1992). The pre-edge peak in the Cu and Co *K*-edge spectra of carrollite is assigned to Cu $1s \rightarrow 3d$ and Co $1s \rightarrow 3d$ transitions, respectively. Peak **a** in both S *K*- and *L*-edge spectra are well aligned, and also approximately correspond to the pre-edge region in the Cu and Co *K*-edge spectra. Hence, peak **a** in the S *K*- and *L*-edge spectra are assigned to transitions of S 1*s* and 2*p* electrons to the S 3*p*- and 3*s*-like states, respectively, mixed into the σ_B^* or σ_A^* bands (or both). The interpretations of peaks **b**, **c**, $\mathbf{d}_1$ and $\mathbf{d}_2$ in the S *K*- and *L*-edge spectra are also similar to those for pyrite, pyrrhotite and the other metal sulfides (Li *et al.* 1994a, b, c). The S *K*- and *L*-edge spectra of carrollite are in good agreement with the model of the qualitative bonding (Goodenough 1968, Vaughan *et al.* 1971) and MO calculations (Vaughan & Tossell 1981) for thiospinels, but provide new experimental information on the bonding and conduction-band structure of carrollite. First, the unoccupied Co and Cu 3*d* crystal-field bands have a large contribution of S 3*p* states and some features of S 3*s* states, and the metal 3*d* electrons are involved in the bonding of the metals with S atoms. Second, the conduction-band minimum, characterized by metal *sp* states (Goodenough 1968, Vaughan *et al.* 1971), has high DOS of S 3*s*- and 3*p*-like states, also indicating strong mixing of the metal *sp* states and S 3*s*- and 3*p*-like states.

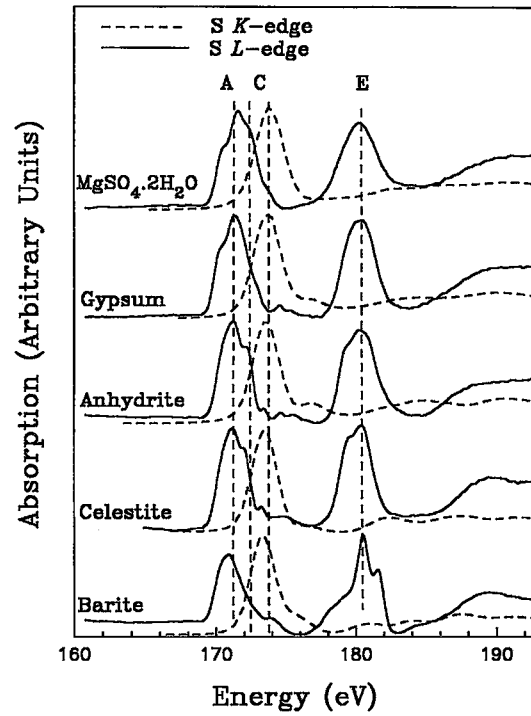

FIG. 4. S *K*-edge (dash curves) and S *L*-edge (solid curves) XANES spectra of synthetic $MgSO_4 \cdot 2H_2O$, gypsum, anhydrite, celestite and barite. The S *K*- and *L*-edge spectra are correlated by the S $K\alpha_1$ X-ray emission energy at 2307.8 eV and the S 1s BE for *K*-edge spectra, and the $2p_{3/2}$ BE for *L*-edge spectra.

TABLE 1. S *K*- AND *L*-EDGE XANES SPECTRA OF SOME SULFATES

Sample	Label	Assignments	*K*-edge* (eV)	*L*-edge* (eV)	Assignments
$MgSO_4$.$2H_2O$	A			170.5	S $2p_{3/2} \rightarrow a_1$ (3*s*-like)
				171.6	S $2p_{1/2} \rightarrow a_1$ (3*s*-like)
	C	S $1s \rightarrow t_2$ (3*p*-like)	2481.5	172.3	S $2p_{3/2} \rightarrow t_2$ (3*p*/3*s*-like)
				173.7	S $2p_{1/2} \rightarrow t_2$ (3*p*/3*s*-like)
	E			181.0	S $2p \rightarrow e$ (3*d*-like)
Gypsum	A			170.3	S $2p_{3/2} \rightarrow a_1$ (3*s*-like)
				171.3	S $2p_{1/2} \rightarrow a_1$ (3*s*-like)
	C	S $1s \rightarrow t_2$ (3*p*-like)	2481.5	172.9	S $2p \rightarrow t_2$ (3*p*/3*s*-like)
	E			180.2	S $2p \rightarrow e$ (3*d*-like)
Anhydrite	A			171.2	S $2p \rightarrow a_1$ (3*s*-like)
	C	S $1s \rightarrow t_2$ (3*p*-like)	2481.3	172.2	S $2p_{3/2} \rightarrow t_2$ (3*p*/3*s*-like)
				173.4	S $2p_{1/2} \rightarrow t_2$ (3*p*/3*s*-like)
	E			179.2	S $2p_{3/2} \rightarrow e$ (3*d*-like)
				180.2	S $2p_{1/2} \rightarrow e$ (3*d*-like)
Celestite	A			171.1	S $2p \rightarrow a_1$ (3*s*-like)
	C	S $1s \rightarrow t_2$ (3*p*-like)	2481.3	172.0	S $2p_{3/2} \rightarrow t_2$ (3*p*/3*s*-like)
				173.2	S $2p_{1/2} \rightarrow t_2$ (3*p*/3*s*-like)
				179.5	S $2p_{3/2} \rightarrow e$ (3*d*-like)
	E			180.4	S $2p_{1/2} \rightarrow e$ (3*d*-like)
Barite	A			170.9	S $2p \rightarrow a_1$ (3*s*-like)
	C	S $1s \rightarrow t_2$ (3*p*-like)	2481.1	173.9	S $2p \rightarrow t_2$ (3*p*/3*s*-like)
	E			180.5	S $2p_{3/2} \rightarrow e$ (3*d*-like)
				181.6	S $2p_{1/2} \rightarrow e$ (3*d*-like)

*The error in the *K*-edge and *L*-edge photon energy measurements is estimated at ±0.1 eV.

Mg, Ca, Sr and Ba sulfates

Figure 4 compares the S *K*- (dash curves) and *L*-edge (solid curves) XANES spectra of $MgSO_4 \cdot 2H_2O$, gypsum ($CaSO_4 \cdot 2H_2O$), anhydrite ($CaSO_4$), celestite ($SrSO_4$) and barite ($BaSO_4$), aligned by the S $K\alpha_1$ X-ray emission energy at 2307.8 eV and the S 1s BE for *K*-edge spectra and $2p_{3/2}$ BE for *L*-edge spectra. The peak positions and assignments are summarized in Table 1. The assignments are based on comparison with the S *K*- and *L*-edge spectra of Na_2SO_4 (Dehmer 1972, Sutherland *et al.* 1993), gaseous SF_4 (Bodeur & Hitchcock 1987) and SO_2Cl_2 (Hitchcock *et al.* 1987), and Si *K*- and *L*-edge spectra of SiF_4 (Friedrich *et al.* 1980) and α-quartz (Li *et al.* 1993). Peak **A** in the *L*-edge spectra is assigned to the transition of S 2*p* electrons to S 3*s*-like a_1 states, and it is split by about 1.2 eV, owing to the spin–orbit interaction of S 2*p* orbitals. Peak **A** is absent in the *K*-edge spectra, because the S $1s \rightarrow 3s$ transition is forbidden by the selection rules. Peak **C** in the *K*-edge spectra is attributed to the transition of S 1*s* electrons to the S 3*p*/3*s*-like t_2 states. Peak **E** is assigned to the S 3*d*-like e and t_2 states, and is weak in the *K*-edge spectra because of the forbidden S $1s \rightarrow 3d$ transitions.

We also observe some systematic changes in the S *K*- and *L*-edge spectra from $MgSO_4 \cdot 2H_2O$ and gypsum to anhydrite, celestite and barite. For $MgSO_4 \cdot 2H_2O$ and gypsum, which contain structurally bound H_2O, peak **A** in the *L*-edge spectra shifts to lower energy, the first peak of this doublet is weaker, and there is no spin–orbit splitting of peak **E**. For anhydrite and celestite, the spin–orbit splitting of peak **E** is resolved. For barite, peak **A** also shifts to lower energy, as for gypsum, but is not discernibly split, whereas peak **E** moves to higher energy and is apparently split by the spin-orbit interaction of S 2*p* orbitals. Peak **C** in the *K*-edge spectra tends to shift to lower energy, and the post-edge features become more complicated from $MgSO_4 \cdot 2H_2O$ to barite, probably related to the greater back-scattering efficiency of the heavier cations beyond the first shell. A second-order Ca *L*-edge doublet is discernible at about 174.6 and 175.4 eV in the *L*-edge spectra of gypsum and anhydrite, and the corresponding Ba doublet appears as the low-energy shoulder to peak **E** in the *L*-edge spectrum of barite.

DISCUSSION

Chemical shifts of S K- and L-edges and oxidation state of sulfur

We have reported S *K*- and *L*-edge XANES spectra of several metal sulfides and sulfate minerals in this study and previous papers (Li *et al.* 1994a, b, c). The first peak in the S *K*- and *L*-edge XANES spectra corresponds to the first unoccupied state. The positions

TABLE 2. S *K*- AND *L*-EDGES, ENERGY BAND GAP (E_g) AND REFLECTIVITY (R %) OF SULFIDES, SULFOSALTS AND SULFATES

Mineral	Formula	*K*-edge* (eV)	*L*-edge* (eV)	E_g (eV)	R (%)	Symbols
Sphalerite	ZnS	2473.4	163.6	3.8	16.4	Sp
Wurtzite	ZnS	2473.2	163.5	3.9	16.3	Wz
Greenockite	CdS	2472.3	162.2	2.5	18.7	Grn
Metacinnabar	HgS	2471.7	162.0	2.3	25.2	Mcin
Orpiment	As_2S_3	2470.8	161.6	2.4	23.1	Op
Realgar	As_4S_4	2471.1	161.8	2.2	19.4	Rg
Cinnabar	HgS	2471.1	161.8	2.0	28.1	Cin
Proustite	Ag_3AsS_3	2471.1	162.0	2.0	29.3	Pro
Stibnite	Sb_2S_3	2470.7	161.7	1.7	38.3	Stb
Molybdenite	MoS_2	2469.4	161.9	1.0	44.0	Mo
Pyrrhotite	$Fe_{1-x}S$	2469.8	161.7	1.0	38.9	Po
Covellite	CuS	2471.1	162.5	2.0	19.3	Cv
Tetrahedrite	$Cu_{12}Sb_4S_{13}$	2470.9	162.1	1.8	33.0	Tet
Stannite	Cu_2FeSnS_4	2470.8	162.3	1.5	29.0	Sta
Chalcocite	Cu_2S	2470.1	162.2	1.1	30.2	Cc
Enargite	Cu_3AsS_4	2470.1	162.0	1.0	26.0	Eng
Bornite	Cu_5FeS_4	2470.0		1.0	24.4	Bn
Cubanite	$CuFe_2S_3$	2469.5	161.6	0.7	40.2	Cub
Chalcopyrite	$CuFeS_2$	2469.6	161.7	0.7	38.8	Ccp
Linnaeite	Co_3S_4	2469.8	161.7		44.7	Lin
Carrollite	$CuCo_2S_4$	2469.7	161.6		41.9	Car
Pyrite	FeS_2	2471.3	163.0	0.9	55.0	Py
Marcasite	FeS_2	2471.2	163.0	0.9	51.6	Mar
Sulfur	S_8	2472.0	163.3			
Na_2SO_3		2477.4	168.6			
Barite	$BaSO_4$	2481.1	170.9			
Celestite	$SrSO_4$	2481.2	171.1			
Anhydrite	$CaSO_4$	2481.3	171.2			
Gypsum	$CaSO_4.2H_2O$	2481.5	171.3			
	$MgSO_4.2H_2O$	2481.6	171.6			
	$MnSO_4$	2481.2	171.8			
	$FeSO_4$	2481.7	171.5			
	$CoSO_4$	2481.5	171.4			
	$NiSO_4$	2481.5	171.5			
	$Na_2S_2O_3$	2479.3	169.5			
		2470.8	162.9			

*The error in the *K*-edge and *L*-edge photon energy measurements is estimated at ± 0.1 eV.

of the first peak of all these materials, together with the band gap, E_g, and reflectivity of metal sulfides, are summarized in Table 2.

Figure 5 shows that the S *K*- and *L*-edges shift toward higher energy in the order from sulfides to sulfite and sulfates, and unambiguously quantitatively distinguish between these oxidation states. The energy shift from S^{2-} to S^{6+} species is about 10 eV for both S *K*- and *L*-edges (Fig. 6).

The chemical shift in the X-ray absorption edge depends on the initial and final states involved in the transition. If a valence electron is removed from an atom, the screening of core electrons by valence electrons is reduced, and the core energy-levels become more tightly bound. Therefore, the binding energy of the inner-shell S 2*p* increases with increase in its oxidation state, as is evident in the XPS chemical shift. On the other hand, comparing S^{n+} compounds and clusters, the more oxidized species of sulfur form a stronger bond with the same ligand, promoting greater overlap of sulfur and ligand orbitals. This gives more stable bonding orbitals, and less stable anti-bonding orbitals. Consequently, the S *K*- and *L*-edges are expected to shift toward higher energy with increase in the oxidation state of sulfur. The correlations in Figure 6 unambiguously determine the

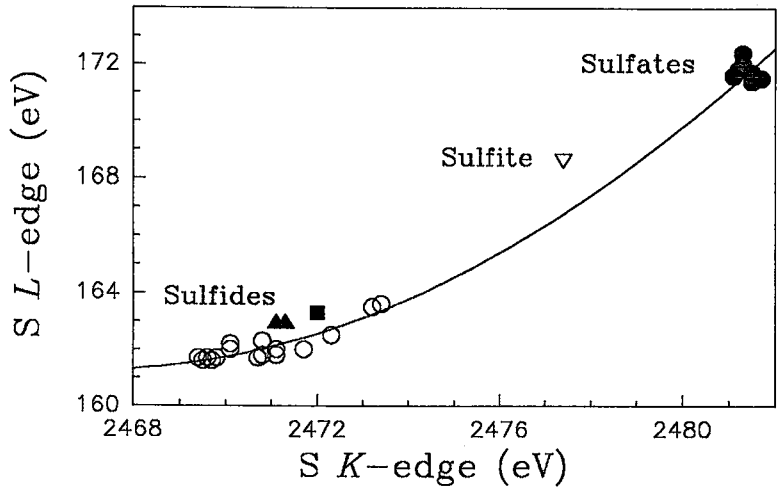

FIG. 5. Correlation of S *K*- and *L*-edges in sulfides (open circles and solid triangles), sulfur (solid square), sulfite (inverted triangle) and sulfates (solid circles). The data used in this figure are listed in Table 2.

oxidation state and form of sulfur in any kind of substance and any state of matter. For example, in sodium thiosulfate ($Na_2S_2O_3$), it is commonly accepted that there are two different sulfur species, S^{2-} and S^{6+}; the S *K*- and *L*-edge XANES spectra of this compound are plotted in Figure 6 as an empty and solid square, respectively. Clearly, one of the sulfur species in $Na_2S_2O_3$ is better described as S^{5+}, and the other one is S^{-}, similar to sulfur in pyrite (Huffman *et al.* 1991, Vairavamurthy *et al.* 1993, 1994).

The shifts of S *K*- and *L*-edges with oxidation state of sulfur are very similar to those of the S 2*p* BE as measured by XPS. Figure 7 shows the correlations (solid circles) of S *K*- and *L*-edges with the S 1*s* and 2*p* BE, respectively. The experimental S *K*- and *L*-edge data are shown as solid circles, and are compared with the ideal correlations for S *K*- and *L*-edge values set equal to the respective S 1*s* and 2*p* BE (open circles and straight lines). The S 2*p* BE were measured by XPS and cited from Hyland & Bancroft (1989) for

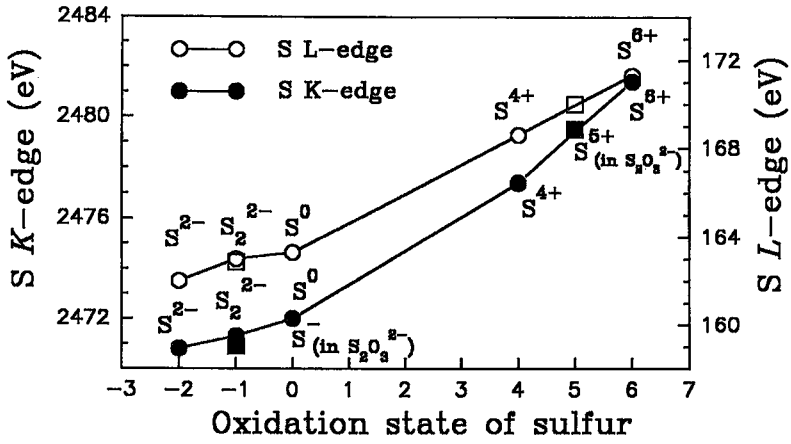

FIG. 6. Variation of S *K*-edge (solid dots, left-hand scale) and S *L*-edge (open circles, right-hand scale) with oxidation state of sulfur. The S *K*-edge (solid squares) and S *L*-edge (open squares) of the two sulfur species in $Na_2S_2O_3$ are also plotted on this diagram, identifying one of the species as S^{5+}, and the other as S^{-}. The S *K*- and *L*-edges for S^{2-} are averages of 22 metal sulfides, and the data for S^{6+} are averages of 10 sulfates (Table 1).

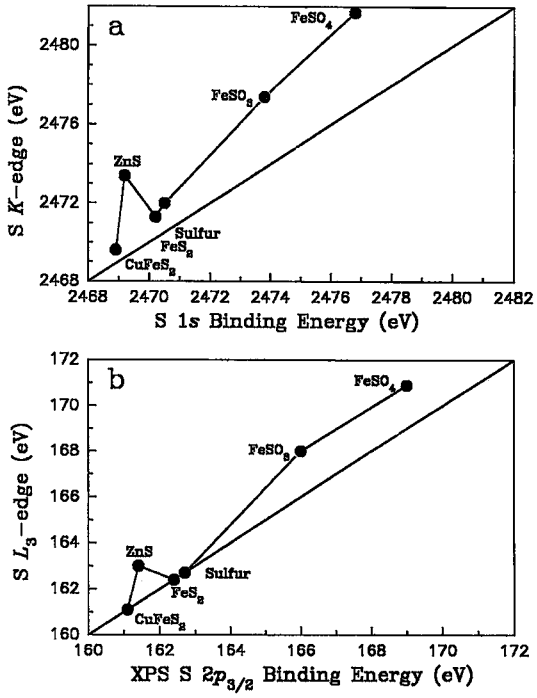

FIG. 7. Correlations between S *K*-edge and S 1*s* BE (a) and S *L*-edge and XPS S $2p_{3/2}$ BE (b) of $CuFeS_2$, ZnS, FeS_2, native sulfur, $FeSO_3$ and $FeSO_4$.

ZnS, FeS_2 and native sulfur, and from Fleet *et al.* (1993) and Richardson & Vaughan (1989) for $FeSO_3$ and $FeSO_4$. The S *K*- and *L*-edge values of $FeSO_3$ are assumed to be equal to those of $NaSO_3$. The S 1s BE was calculated by adding the S 2*p* BE and the S $K\alpha_1$ X-ray emission energy at 2307.8 eV. In general, the S *K*-edge and S 1*s* BE, as well as the S *L*-edge and S 2*p* BE, shift toward higher energy with oxidation state of sulfur. However, the shifts of S *K*- and *L*-edges are larger, because they depend on the shifts of the unoccupied final states, as well as the BE of the inner shells. It is very difficult to quantitatively evaluate the contributions of the initial and final states to the shifts of S *K*- and *L*-edges. However, as shown in Figure 7, the BE shifts of S 1*s* and 2*p* mainly contribute to the S *K*- and *L*-edge shifts, but the shifts of the final states also make some contribution. As an example, the S 2*p* BE of ZnS and $CuFeS_2$, both of which contain S^{2-}, are very similar, but the S *K*- and *L*-edges of ZnS shift to much higher energy than those of $CuFeS_2$. Therefore, the shifts of the final unoccupied states *must* make a significant contribution to the edge positions.

Chemical shifts of S K- and L-edges versus the E_g and reflectivity of metal sulfides

Figure 8 shows a positive linear correlation between the S *K*- and *L*-edges of metal sulfides; even for metal sulfides containing only S^{2-}, the S *K*- and *L*-edges also shift significantly. Although small differences probably exist owing to different geometrical and electronic structures, the inner 1*s* and 2*p* shells must be very similar for different sulfides. Clearly, the chemical shifts in the S *K*- and *L*-edges depend mainly on the final states, that is, the first unoccupied states. The first unoccupied states are the metal 3*d* band mixed with S 3*s*- and 3*p*-like states in the band gap for transition metal (Fe, Co, Ni, Cu and Mo) sulfides, and are antibonding S 3*s*- and 3*p*-like states at the conduction-band minimum for Zn, Cd, Hg, As and Sb sulfides with fully occupied *d* orbitals. Therefore, both S *K*- and *L*-edges are at a lower energy for the former (empty circles), and move to higher energy for the latter (filled circles). The chemical shifts in the S *K*- and *L*-edges are related to the crystal chemistry,

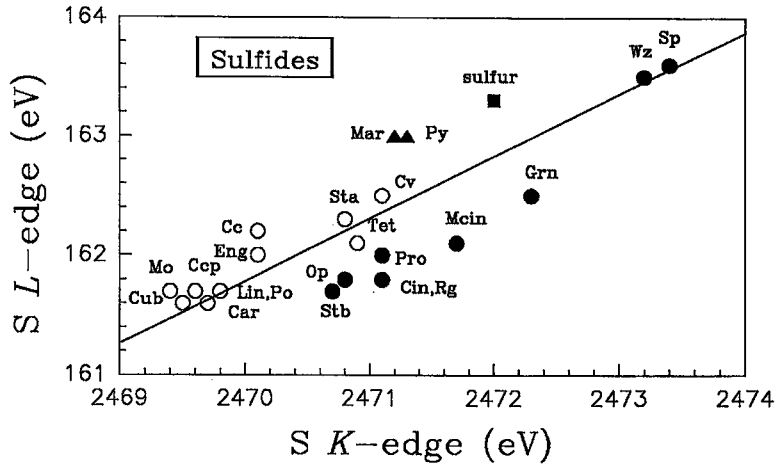

FIG. 8. Correlation of the S *K*- and *L*-edge positions of metal sulfides. Abbreviations of mineral names are keyed to Table 2.

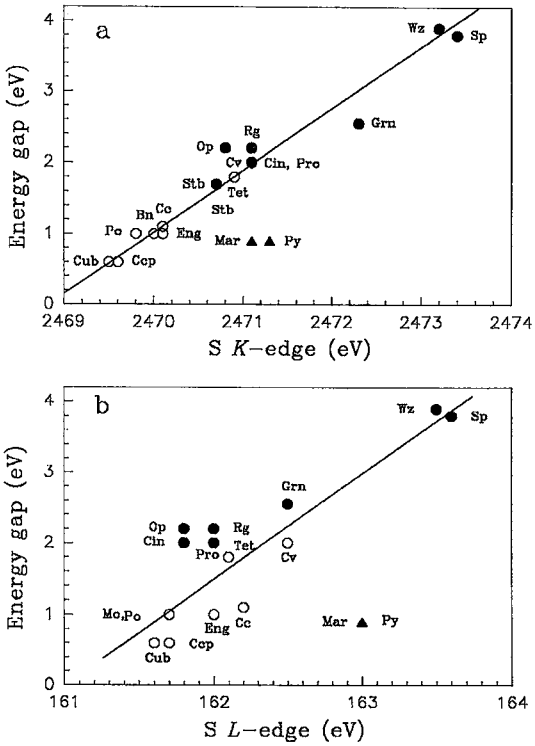

FIG. 9. Correlation of S *K*-edge (a) and S *L*-edge (b) with energy band gap (E_g) of metal sulfides. The E_g values are from Shuey (1975), and abbreviations of mineral names are keyed to Table 2.

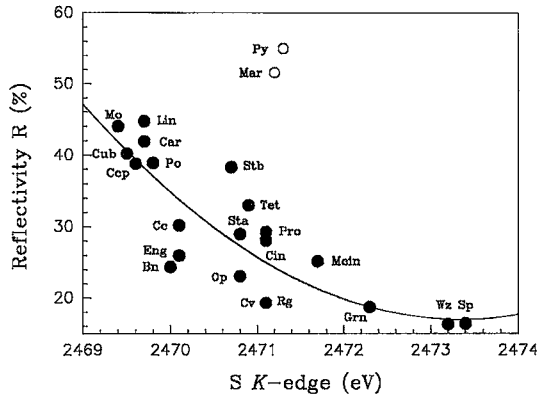

FIG. 10. Correlation of reflectivity with S *K*-edge for metal sulfides. The reflectivity values are from Anthony *et al.* (1990), with abbreviations of mineral names keyed to Table 2.

electronic structure, E_g and reflectivity of these semiconducting materials.

Figure 9 shows the correlation of the S *K*- and *L*-edges with the E_g of metal sulfides, where the E_g data are mainly from Shuey (1975) and were estimated from optical spectra. First, it is apparent that for transition-metal sulfides that have small electrical resistance (Vaughan & Craig 1978), both S *K*- and *L*-edges lie at lower energy, and the band gap is smaller. For Zn, Cd, Hg, As and Sb sulfides, which usually have higher electrical resistance (Vaughan & Craig 1978), the band gap is larger, and both S *K*- and *L*-edges are also at a higher energy. Second, for all sulfides studied, both S *K*- and *L*-edges are linearly correlated with E_g. In general, the correlations of S *K*- and *L*-edges with the band gap of metal sulfides seem quite acceptable because some of the small deviations from linearity are probably due to the present use of approximate E_g values. Thus, the data in Figure 9 indicate that the first unoccupied S 3*s*- or 3*p*-like states in the sulfides increase in energy with increase in E_g. These linear correlations establish a potential application of S *K*- and *L*-edge spectra in the determination of E_g in semiconducting metal sulfides. Figure 10 shows the correlation of the S *K*-edge position with the reflectivity *R* (%) of these metal sulfides, where the reflectivity values are cited from Anthony *et al.* (1990). Pyrite and marcasite depart from the correlations of Figures 9 and 10, presumably because they contain S_2^{2-} species, rather than simple S^{2-} species.

ACKNOWLEDGEMENTS

We thank F.C. Hawthorne and an unnamed referee for helpful comments, D. Dillon, F.J. Wicks, T. Ottoway and R. Ramik for provision of mineral samples. This study was supported by NSERC. We also thank the staff at the Synchrotron Radiation Center (SRC), the University of Wisconsin for their technical assistance, and the National Science Foundation (NSF) for the support of the SRC.

REFERENCES

ANTHONY, J.W., BIDEAUX, R.A., BLADH, K.W. & NICHOLS, M.C. (1990): *Handbook of Mineralogy. I. Elements, Sulfides and Sulfosalts.* Mineral Data Publishing, Tucson, Arizona.

BANCROFT, G.M. (1992): New developments in far UV, soft X-ray research at the Canadian synchrotron radiation facility. *Can. Chem. News* **44**(6), 15-22.

BODEUR, S. & HITCHCOCK, A.P. (1987): Inner- and valence-shell excitation of SF_4 studied by photoabsorption and electron energy loss spectroscopy. *Chem. Phys.* **111**, 467-479.

BROWN, G.E., JR. (1990): Spectroscopic studies of chemisorption reaction mechanisms at oxide–water interfaces. *Rev. Mineral.* **23**, 309-364.

_____, CALAS, G., WAYCHUNAS, G.A. & PETIAU, J. (1988): X-ray absorption spectroscopy and its applications in mineralogy and geochemistry. *Rev. Mineral.* **18**, 431-512.

_____ & PARKS, G.A. (1989): Synchrotron-based X-ray absorption studies of cation environments in Earth materials. *Rev. Geophys.* **27**, 519-533.

_____, _____ & CHISHOLM-BRAUSE, C.J. (1989): In situ X-ray absorption spectroscopic studies of ions at oxide–water interfaces. *Chimia* **43**, 248-256.

BULLETT, D.W. (1982): Electronic structure of 3*d* pyrite- and marcasite-type sulphides. *J. Phys. C: Solid State Phys.* **15**, 6163-6174.

CALAS, G., BASSETT, W.A., PETIAU, J., STEINBERG, M., TCHOUBAR, D. & ZARKA, A. (1984): Some mineralogical applications of synchrotron radiation. *Phys. Chem. Minerals* **11**, 17-36.

_____, BROWN, G.E., JR., WAYCHUNAS, G.A. & PETIAU, J. (1987): X-ray absorption spectroscopic studies of silicate glasses and minerals. *Phys. Chem. Minerals* **15**, 19-29.

CHARNOCK, J., GARNER, C.D., PATTRICK, R.A.D. & VAUGHAN, D.J. (1990): An EXAFS study of thiospinel minerals. *Am. Mineral.* **75**, 247-255.

DEHMER, J.L. (1972): Evidence of effective potential barriers in the X-ray absorption spectra of molecules. *J. Chem. Phys.* **56**, 4496-4504.

DRÄGER, G., FRAHM, R., MATERLIK, G. & BRÜMMER, O. (1988): On the multiple character of the X-ray transitions in the pre-edge structure of Fe *K* absorption spectra: an experimental study. *Phys. Status Sol.* **B146**, 287-294.

FLEET, M.E., CHRYSSOULIS, S.L., MACLEAN, P.J., DAVISON, R. & WEISENER, C.G. (1993): Arsenian pyrite from gold deposits: Au and As distribution investigated by SIMS and EMP, and color staining and surface oxidation by XPS and LIMS. *Can. Mineral.* **31**, 1-17.

FRIEDRICH, H., PITTEL, B., RABE, P., SCHWARZ, W.H.E. & SONNTAG, B. (1980): Overlapping core to valence and core to Rydberg transition and resonances in the XUV spectra of SiF_4. *J. Phys. B: Atoms Molec. Phys.* **13**, 25-30.

GOODENOUGH, J.B. (1968): Description of outer *d* electrons in thiospinels. *J. Phys. Chem. Solids* **30**, 261-280.

_____ (1972): Energy bands in TX_2 compounds with pyrite, marcasite, and arsenopyrite structures. *J. Solid State Chem.* **5**, 144-152.

HITCHCOCK, A.P., BODEUR, S. & TRONC, M. (1987): Sulfur and chlorine *K*-shell X-ray absorption spectra of SCl_2, S_2Cl_2, $SOCl_2$ and SO_2Cl_2. *Chem. Phys.* **115**, 93-101.

HUFFMAN, G.P., MITRA, S., HUGGINS, F.E., SHAH, N., VAIDYA, S. & LU, FULONG (1991): Quantitative analysis of all major forms of sulfur in coal by X-ray absorption fine structure spectroscopy. *Energy Fuels* **5**, 574-581.

HYLAND, M.M. & BANCROFT, G.M. (1989): An XPS study of gold deposition at low temperatures on sulfide minerals: reducing agents. *Geochim. Cosmochim. Acta* **53**, 367-372.

KITAMURA, M., SUGIURA, C. & MURAMATSU, S. (1988): Multiple-scattering calculation of sulfur K X-ray absorption spectra for FeS, CoS and NiS. *Solid State Commun.* **67**, 313-316.

KOSSEL, W.V. (1920): Zum Bau der Rontgenspektren. *Z. Phys.* **1**, 119-134.

LI, DIEN, BANCROFT, G.M., KASRAI, M., FLEET, M.E., FENG, XINGHONG, TAN, KIM & YANG, B.X. (1993): High-resolution Si *K*- and $L_{2,3}$-edge XANES of α-quartz and stishovite. *Solid State Commun.* **87**, 613-617.

_____, _____, _____, _____, _____, _____ & _____ (1994a): Sulfur *K*- and *L*-edge XANES and electronic structure zinc, cadmium and mercury monosulfides: a comparative study. *J. Phys. Chem. Solids* **55**, 535-543.

_____, _____, _____, _____, _____, YANG, B.X. & TAN, KIM (1994b): S *K*- and *L*-edge XANES and electronic structure of some copper sulfide minerals. *Phys. Chem. Minerals* **21**, 317-324.

_____, _____, _____, _____, YANG, B.X., FENG, XINGHONG, TAN, KIM & PENG, M. (1994c): Sulfur *K*- and *L*-edge X-ray absorption spectroscopy of sphalerite, chalcopyrite and stannite. *Phys. Chem. Minerals* **20**, 489-499.

NAKAI, I., SUGITANI, Y., NAGASHIMA, K. & NIWA, Y. (1978): X-ray photoelectron spectroscopic study of copper minerals. *J. Inorg. Nucl. Chem.* **40**, 789-791.

RICHARDSON, S. & VAUGHAN, D.J. (1989): Surface alteration of pentlandite and spectroscopic evidence for secondary violarite formation. *Mineral. Mag.* **53**, 213-222.

SAKKOPOULOS, S., VITORATOS, E. & ARGYREAS, T. (1984): Energy-band diagram for pyrrhotite. *J. Phys. Chem. Solids* **45**, 923-928.

SAYERS, D.E., LYTLE, F.W. & STERN, E.A. (1970): Point scattering theory of X-ray *K* absorption fine structure. *Adv. X-ray Anal.* **13**, 248-271.

SHUEY, R.T. (1975): *Semiconducting Ore Minerals*. Elsevier, Amsterdam, The Netherlands.

STERN, E.A. (1974): Theory of the extended X-ray absorption fine structure. *Phys. Rev.* **B10**, 3027-3037.

_____, SAYERS, D.E. & LYTLE, F.W. (1975): Extended X-ray absorption fine structure technique. III. Determination of physical parameters. *Phys. Rev.* **B11**, 4836-4846.

SUGIURA, C. (1981): Sulfur *K* X-ray absorption spectra of FeS, FeS_2, and Fe_2S_3. *J. Chem. Phys.* **74**, 215-217.

_____ (1984): Iron *K* X-ray absorption-edge structures of FeS and FeS_2. *J. Chem. Phys.* **80**, 1047-1049.

_____, GOHSHI, Y. & SUZUKI, I. (1974): Sulfur K_β X-ray emission spectra and electronic structures of some metal sulfides. *Phys. Rev.* **B10**, 338-343.

_____ & MURAMATSU, S. (1985): Sulfur *K* X-ray absorption-edge structures and electronic states of transition-metal sulfides MS and MS_2 (M = Fe, Co, Ni). *Phys. Stat. Sol.* **B129**, K157-K161.

SUTHERLAND, D.G.J., KASRAI, M., BANCROFT, G.M., LIU, Z.F. & TAN, KIM (1993): Si *L*- and *K*-edge X-ray-absorption near-edge spectroscopy of gas-phase $Si(CH_3)_x(OCH_3)_{4-x}$: models for solid-state analogs. *Phys. Rev.* **B48**, 14,989-15,001.

TOSSELL, J.A. (1977): SCF–X_α scattered wave MO studies of the electronic structure of ferrous iron in octahedral coordination with sulfur. *J. Chem. Phys.* **66**, 5712-5719.

_____ & VAUGHAN, D.J. (1992): *Theoretical Geochemistry: Application of Quantum Mechanics in the Earth and Mineral Sciences.* Oxford University Press, New York, N.Y.

_____, _____ & BURDETT, J.K. (1981): Pyrite, marcasite, and arsenopyrite type minerals: crystal chemical and structural principles. *Phys. Chem. Minerals* **7**, 177-184.

VAIRAVAMURTHY, A., MANOWITZ, B., LUTHER, G.W., III & JEON, Y. (1993): Oxidation states of sulfur in thiosulfate and implications for anaerobic energy metabolism. *Geochim. Cosmochim. Acta* **57**, 1619-1623.

_____, _____, ZHOU, WEIQING & JEON, Y. (1994): Determination of hydrogen sulfide oxidation products by sulfur *K*-edge X-ray absorption near-edge structure spectroscopy. *In* Environmental Geochemistry of Sulfide Oxidation (C.N. Alpers & D.W. Blowes, eds.). *Am. Chem. Soc., Symp. Ser.* **550**, 412-430.

VAUGHAN, D.J., BURNS, R.G. & BURNS, V.M. (1971): Geochemistry and bonding of thiospinel minerals. *Geochim. Cosmochim. Acta* **35**, 365-381.

_____ & CRAIG, J.R. (1978): *Mineral Chemistry of Metal Sulfides.* Cambridge University Press, Cambridge, U.K.

_____ & TOSSELL, A.J. (1981): Electronic structure of thiospinel minerals: results from MO calculations. *Am. Mineral.* **66**, 1250-1253.

WELZ, D. & ROSENBERG, M. (1987): Electronic band structure of tetrahedral iron sulfides. *J. Phys. C: Solid State Phys.* **20**, 3911-3924.

YANG, B.X., MIDDLETON, F.H., OLSSON, B.G., BANCROFT, G.M., CHEN, J.M., SHAM, T.K., TAN, KIM & WALLACE, D.J. (1992): The design and performance of a soft X-ray double crystal monochromator beamline at Aladdin. *Nucl. Inst. Methods Phys. Res.* **A316**, 422-436.

Received November 28, 1994, revised manuscript accepted May 23, 1995.